Published in final edited form as:
Clin Neurophysiol. 2004 December ; 115(12): 2718–2727.

Quantitative visualization of ictal subdural EEG changes in children with neocortical focal seizures

Eishi Asano[a,b,*], **Otto Muzik**[a,b,c], **Aashit Shah**[b], **Csaba Juhász**[a,b], **Diane C. Chugani**[a,b,c], **Kenji Kagawa**[a], **Krisztina Benedek**[a], **Sandeep Sood**[d], **Jean Gotman**[e], and **Harry T. Chugani**[a,b,c]

a *Department of Pediatrics, Children's Hospital of Michigan, Wayne State University, Detroit, MI 48201, USA*

b *Department of Neurology, Children's Hospital of Michigan, Wayne State University, Detroit, MI 48201, USA*

c *Department of Radiology, Children's Hospital of Michigan, Wayne State University, Detroit, MI 48201, USA*

d *Department of Neurosurgery, Children's Hospital of Michigan, Wayne State University, Detroit, MI 48201, USA*

e *Department of Neurology, Montreal Neurological Institute and Hospital, McGill University, Montreal, Que., Canada H3A 2B4*

Abstract

Objective—To quantify the ictal subdural electroencephalogram (EEG) changes using spectral analysis, and to delineate the quantitatively defined ictal onset zones on high-resolution 3D MR images in children with intractable neocortical epilepsy.

Methods—Fourteen children with intractable neocortical epilepsy (age: 1–16 years) who had subsequent resective surgery were retrospectively studied. The subjects underwent a high-resolution MRI and prolonged subdural EEG recording. Spectral analysis was applied to 3 habitual focal seizures. After fast Fourier transformation of the EEG epoch at ictal onset, an amplitude spectral curve (square root of the power spectral curve) was created for each electrode. The EEG magnitude of ictal rhythmic discharges was defined as the area under the amplitude spectral curve within a preset frequency band including the ictal discharge frequency, and calculated for each electrode. The topography mapping of ictal EEG magnitude was subsequently displayed on a surface-rendered MRI. Finally, receiver operating characteristic (ROC) analysis was performed to evaluate the consistency between quantitatively and visually defined ictal onset zones.

Results—The electrode showing the maximum of the averaged ictal EEG magnitude was part of the visually defined ictal onset zone in all cases. ROC analyses demonstrated that electrodes showing >30% of the maximum of the averaged ictal EEG magnitude had a specificity of 0.90 and a sensitivity of 0.74 for the concordance with visually defined ictal onset zones.

Significance—Quantitative ictal subdural EEG analysis using spectral analysis may supplement conventional visual inspection in children with neocortical epilepsy by providing an objective definition of the onset zone and its simple visualization on the patient's MRI.

* Corresponding author. Address: Division of Pediatric Neurology, Children's Hospital of Michigan, Wayne State University, 3901 Beaubien Street, Detroit, MI 48201, USA. Tel.: +1-313-745-5547; fax: +1-313-745-0955. *E-mail address:* eishi@pet.wayne.edu (E. Asano)..

Keywords

Clinical neurophysiology; Pediatric epilepsy surgery; Quantitative ictal intracranial electroencephalography; Focal cortical dysplasia; Tuberous sclerosis complex

1. Introduction

Epileptic seizures are represented as synchronized and sustained rhythmic ictal discharges with certain frequencies on the electroencephalogram (EEG). The ictal EEG onset on subdural electrodes is commonly used in defining the presumed epileptic focus (Lüders et al., 1993), resection of which is an effective treatment for selected patients with drug-resistant focal epilepsy of neocortical origin. However, the definition of ictal onset zones is subjective and varies among electroencephalographers, and ictal EEG changes are often brief and widespread in children. To define the ictal onset zone more precisely and objectively, various quantitative methods have been applied to preictal as well as ictal subdural EEG recordings (Alarcon et al., 1995; Chen et al., 2002; Gotman et al., 1993; Otsubo et al., 2001; Sun et al., 2001). Spectral analysis remains an integral part of digital signal processing technology, and previous studies using spectral analysis demonstrated a general concordance between quantitatively and visually defined ictal subdural EEG onset zones in adults with temporal lobe epilepsy (Alarcon et al., 1995; Gotman et al., 1993). In the present study of children with neocortical epilepsy, we quantified the ictal subdural EEG changes using spectral analysis and delineated the quantitatively defined ictal onset zones on high-resolution 3D MR images. We subsequently determined whether the quantitatively defined ictal onset zone was consistent with the ictal onset zone determined by visual analysis.

2. Methods

2.1. Patients

Fourteen children (11 boys and 3 girls; ages: 1–16 years) with drug-resistant focal seizures of neocortical origin confirmed by at least 3 ictal events recorded by subdural EEG were retrospectively studied (Table 1). The subjects underwent scalp video-EEG monitoring, MRI, glucose metabolism positron emission tomography (PET), and chronic subdural EEG monitoring with subdural electrodes as part of their presurgical evaluation. On MRI, two children showed cortical tubers, two children had a brain tumor, and one child each had subcortical heterotopias, pachygyria, polymicrogyria, polencephaly, and old cerebral infarction due to meningitis. In the remaining 5 children, MRI was normal but glucose metabolism PET scan showed neocortical hypometabolic regions in the presumed epileptic hemisphere. Two patients had previous resective surgery (patients #11 and 14; Table 1). Five children (patients #2, 9, 10, 12 and 14) had a history of secondary generalized tonic clonic seizures in addition to focal seizures. None of the subjects had a history of epileptic spasms.

Resective surgery was performed according to the visually defined subdural EEG data described below. In all patients except patient #4, cortical resection included brain regions showing ictal onset, rapid seizure spread and frequent interictal spike bursts in addition to structural lesions delineated by neuroimaging techniques, while eloquent areas were spared based on results of functional mapping. Although ictal discharges quickly involved the parieto-temporal regions, patient #4 had left frontal lobectomy without additional parietal or temporal resection, since seizure semiology and glucose metabolism PET results strongly suggested pure frontal lobe seizures. Following resective surgery, 10 children became seizure-free, one child had rare seizures (patient #3), two children (patients #8 and 13) had at least 90% reduction of seizure frequency, and another child (patient #5) had 50% reduction of seizure frequency (mean follow-up: 18 months [range: 8–27 months]).

2.2. Subdural electrode placement

For chronic subdural EEG recording, platinum grid electrodes (10 mm intercontact distance) were surgically implanted. The total number of electrode contacts in each subject ranged from 56 to 120. The placement of subdural electrodes was guided by the results of ictal scalp EEG recording, seizure semiology, MRI and interictal glucose metabolism PET. The primary sensory-motor cortex was also covered with electrodes for subsequent functional mapping, if the abnormalities appeared to be close to this region. The medial frontal and temporal regions were covered, when a diagnostic modality suggested possible epileptogenicity in these regions. Every electrode plate was stitched to adjacent plates and/or the edge of dura mater, to avoid movement of subdural electrodes after placement. In addition, intraoperative photographs were taken with a digital camera before dural closure.

2.3. Visual analysis of ictal subdural EEG data

Subdural EEG recordings were obtained using a 128-channel Stellate HARMONIE 5.0 digital system (sampling rate: 200 Hz; Stellate Systems, Inc., Montreal, Que., Canada), for 2–5 days. Medications were tapered and discontinued as necessary to allow seizure capture and subsequent ictal EEG data analysis. At least 3 habitual seizures were captured for visual analysis of ictal EEG findings. Ictal EEG recordings were visually reviewed in the referential and bipolar montages by two electroencephalographers (EA and AS), who obtained a consensus for each electrode to determine whether it should be classified as being part of the seizure-onset zone. Seizure onset was defined as a sustained rhythmic change in the EEG accompanied by subsequent clinically typical seizure activity, not explained by level of arousal, and clearly distinguished from background EEG and interictal activity (Lee et al., 2000; Spencer et al., 1992). Some types of initial EEG changes before seizure onset including brief bursts of spikes and periodic spikes at a frequency of <2 Hz were not considered part of seizure onset for this analysis, according to the concept described by Lee et al. (2000), who reported that brief bursts of spikes and slow periodic spikes are often seen interictally without clinical symptoms and do not necessarily indicate epileptic seizures. Therefore, when such phenomena were the initial EEG changes, we defined the ictal onset electrodes based on the subsequently evolving rhythmic discharge (Lee et al., 2000).

2.4. MRI scanning protocol

MRI studies were performed on a GE Signa 1.5 T scanner (GE Medical Systems, Milwaukee, WI). Anatomical/volumetric imaging of the whole brain was performed in all patients utilizing a T_1-weighted spoiled gradient echo (SPGR) sequence. The 3D SPGR sequence (repetition time [TR] 35 ms; echo time [TE] 5 ms; flip angle, 35°; slice thickness, 1.5 mm; field of view 240 mm) was acquired in the coronal plane.

2.5. Determination of electrode positions on brain surface

In order to reconstruct surface views corresponding to the planar X-ray image (von Stockhausen et al., 1997), 3 virtual markers were defined in the SPGR MR image volume at the same position as in the planar X-ray image. A planar X-ray image was acquired with the subdural electrodes in place for determining the location of the electrodes on the brain surface, while 3 metallic fiducial markers were also placed at anatomically well-defined locations on the patient's head. The 3 locations were the ear lobe and the outer eye corner on the side of the electrodes, and the upper attachment point of the ear to the skull on the contralateral side. The skin was then surface rendered showing details of the ears and the scalp to allow accurate placement of the virtual markers on the 3D-reconstructed MRI. The coordinates of the fiducial markers were also identified on the digital X-ray images. Subsequently, starting from a lateral view of the brain surface, an iterative algorithm was used to minimize the differences between the two sets of coordinate triplets by adjusting the 3 Euler-angles as well as the image zoom,

using the software package '3D TOOL' (Max-Planck-Institute, Cologne, Germany) (von Stockhausen et al., 1997). As a result, a surface view was created which corresponds to the planar X-ray image position and where the location of electrodes was directly defined on the brain surface (Fig. 1F). The accuracy of this procedure was reported previously as 1.24±0.66 mm with a maximal misregistration of 2.7 mm (von Stockhausen et al., 1997). The accuracy of this co-registration process was further enhanced by using intraoperative digital photographs showing in situ locations of the subdural electrodes (Wellmer et al., 2002). Anatomical landmarks (central sulcus, Sylvian fissure, and gyral pattern) that were well identifiable on both the photographs and the 3D-reconstructed brain surface were used to verify the exact location of the electrodes. Following co-registration of the subdural EEG grid with the surface view, virtual spheres with 5 mm diameter were created at those locations on the brain surface, to represent a projection of the electrodes onto the surface. These spheres permanently mark the position of the electrodes on the cortical surface and allow the assessment of electrode grid location relative to the MRI abnormalities from varying view angles.

2.6. Quantitative ictal subdural EEG analysis

Prior to the beginning of subdural EEG monitoring, electrode positions (*x*- and *y*-axis values) on the planar X-ray coordinate were obtained for every electrode using Adobe Photoshop 6.0 (Adobe Systems Incorporated, San Jose, CA), and were registered into the Stellate digital system. Following this procedure, the topographic map derived from the X-ray image can demonstrate the sequential change of EEG signal as well as the ictal EEG magnitude described below (Fig. 1E), since the subdural electrode positions for the EEG topography and 3D-reconstructed MRI were derived from the common planar X-ray image.

Three seizure events, which were least, contaminated with artifacts, as assessed visually, were selected from each patient. If a patient had multiple types of seizures, 3 events of each type of seizures were selected. For each seizure file, the Fast Fourier Transform was calculated for each channel for consecutive preset epochs using the Stellate SENSA 5.0 software. To increase the signal to noise ratio and to maintain the temporal resolution, epoch length was determined so that each epoch contained 10–20 ictal waves, according to the ictal discharge frequency at the first epoch (Fig. 1A). Initially, the frequency of ictal discharge was estimated using the statistics cursor included in the Stellate SENSA software. Thereby, epoch length was set to 5.12, 2.56, 1.28, 0.64, and 0.32 s, when the ictal discharge frequency at the first epoch ranged from 2–4, 4–8, 8–16, 16–32, and >32 Hz, respectively. The above-mentioned epoch lengths have a frequency resolution of 0.19, 0.39, 0.78, 1.56 and 3.13 Hz, respectively. Therefore, a very short epoch length such as 0.32 s is not suitable for analysis of a narrow frequency band such as 2–4 Hz but suitable for analysis of ictal fast wave bursts with a wide frequency range which propagates to other lobes within a second (Jenssen et al., 2002). On the other hand, a longer epoch length such as 5.12 s is suitable for a delta wave onset pattern which takes much longer to propagate to other lobes. The first epoch was placed at the very beginning of the visually defined ictal EEG onset. The spectral analysis was applied to ictal EEG data in the referential montage. If visual inspection revealed that the extracranial reference at the contralateral mastoid was affected by movement artifacts at ictal onset even in the recordings least contaminated with artifacts, the most inactive intracranial electrode distant from the ictal onset zone was used as reference (patient #6).

Following the placement of consecutive epochs, a Fast Fourier Transformation created an amplitude spectrum (*x*-axis unit: Hz; *y*-axis unit: μV/Hz), which is a square root of the power spectrum as computed by way of the Fourier coefficients (*x*-axis unit: Hz; *y*-axis unit: μV^2/Hz), for each epoch and each channel (Fig. 1B–D). The amplitude spectrum ensures a more Gaussian distribution of exported values and is easier to visually relate to the raw EEG record than is the power spectrum (da Silva, 1999). Subsequently, the ictal discharge frequency at the

first epoch was determined for each ictal event, based on the primary peak of the amplitude spectral curve for the first epoch in the most-consistent onset electrode (Fig. 1A and B). Smoothing was applied to the spectral graph, as necessary, for a smoother visual representation of spectral peak (Gotman et al., 1995).

The software subsequently displayed the ictal EEG magnitude (unit: μV) at the first epoch within preset frequency bands, which was calculated as the summation of all frequency components under the amplitude spectral curve within the given frequency band. The frequency bands were preset as follows: 2–4, 4–8, 8–12, 12–16, 16–24, 24–32, 32–88 Hz. The ictal EEG magnitude of 32–88 Hz was calculated without a 56–64 Hz component, if visual inspection revealed a 60 Hz artifact peak on the amplitude spectral curve throughout the entire subdural electrodes. The ictal EEG magnitude at the first epoch within a specific frequency band, that included the ictal discharge frequency, was displayed on the electrode map (Fig. 1E). Thereby, the exported values of EEG magnitude were derived from the amplitude spectral curve without smoothing.

2.7. Statistical analysis

Initially, an ‘averaged interictal EEG magnitude’ was obtained for each channel as a control. A total of 40 epochs clearly representing the interictal state were selected from the sections at least 1 h before the ictal onset and at least 1 h after the seizure offset. Thereby, the interictal epochs were selected from the awake EEG segments in patients who had seizures during awake state and from the sleep EEG segments in those who had seizures during sleep. The interictal EEG magnitude within the same frequency band was calculated for each channel and averaged among 40 interictal epochs, and this calculation yielded an averaged interictal EEG magnitude.

The quantitatively defined ictal EEG onset was defined as electrodes showing the ictal EEG magnitude exceeding two standard deviations from the mean of the averaged interictal EEG magnitude as well as a certain cutoff threshold determined by a receiver operating characteristics (ROC) analysis. To determine whether the quantitatively defined ictal EEG onset was consistent with ‘visually defined onset’ zone, the ROC analysis was performed with the ‘averaged ictal EEG magnitude’ as the predictor and the visually defined onset as the conventional gold standard characterizing true positive (TP = visually defined onset electrode) and true negative (TN = visually defined non-onset electrodes) cases. Thereby, the averaged ictal EEG magnitude was defined as the EEG magnitude at the first epoch within the specific preset frequency band (including the ictal discharge frequency at the first epoch) averaged among 3 seizures. If distinct onset patterns were seen in a single individual, averaged ictal EEG magnitude was created for each ictal onset pattern.

Sensitivity and specificity were computed as follows:

Sensitivity = TP/PC, Specificity = TN/NC

where PC represents all positive cases and NC all negative cases. ROC analysis was repeated for each individual patient. Electrodes showing artifacts were excluded from statistical analysis.

2.8. Topographic display of the sequential changes of the ictal EEG activity

The changes of ictal EEG magnitudes within multiple preset frequency bands described above were sequentially followed until the third epoch, using the same epoch length as the original one. If spectral curves suggested that ictal discharge frequency remained stationary in subsequent epochs, the sequential change of the EEG magnitude within the same frequency band was delineated on the topographic mapping. EEG magnitudes for multiple frequency bands including the primary and secondary spectral peaks were delineated on the topographic

mapping, if (1) visual inspection revealed a recruitment of rhythmic discharges distinct from the ictal onset, (2) another spectral peak evolved at a frequency band different from the original one and (3) its ictal EEG magnitude exceeded two standard deviations from the mean of its averaged interictal EEG magnitude (Fig. 2).

3. Results

Ictal EEG showed rhythmic slow wave onset at delta or theta range in 4 children; rhythmic sinusoidal or sharp wave bursts at alpha frequency in 3 children; fast wave bursts at beta to gamma range in 8 children; and rhythmic spike-wave onset at delta range in one child. Patient #11 had two multifocal foci (fast wave bursts at beta range and rhythmic delta wave onset), and patient #14 also had two multifocal foci (fast wave bursts at gamma range and rhythmic alpha onset). Patient #5 had 3 multifocal foci all of which were represented as rhythmic spike-wave onset at delta range. None of the patients showed rhythmic slow wave onset slower than 2 Hz or a build-up of periodic spike activity at a frequency of <2 Hz without evolution into a continuous rhythmic activity. Regardless of ictal EEG onset pattern, the ictal EEG magnitude for each seizure could be delineated on the 3D-reconstructed MRI (Figs. 1 and 2).

3.1. Statistical results

We first evaluated the sensitivity of the method to the positioning of the first epoch and then to the choice of reference electrode. The spatial pattern (throughout the entire subdural electrode set) of EEG magnitudes within the frequency band including ictal discharge frequency derived from the epoch placed at the visible onset was highly similar to those derived from the epoch placed 50 ms before (mean Spearman's rho=0.98; $P<0.001$) and 50 ms after the visible ictal onset (mean Spearman's rho=0.97; $P<0.001$). Similarly, that same spatial pattern derived from the recording using the intracranial reference was highly similar to that using the extracranial reference (mean Spearman's rho=0.94; $P<0.001$) in the 13 patients whose ictal EEG recordings showed negligible movement artifacts at the extracranial reference. In patient #5 showing spike-wave EEG onsets at delta range in 3 distinct foci, a high similarity was confirmed between the spatial pattern of ictal EEG magnitudes derived from the frequency band including the primary spectral peak at delta range only (2–4 Hz) and that including both the primary and secondary spectral peaks (2–4 and 4–8 Hz) (mean Spearman's rho=0.97; $P<0.001$). Therefore, further statistical analysis for patient #5 was performed using the ictal EEG magnitudes derived from the frequency band solely including the primary spectral peak, as performed in the remaining patients.

The electrode showing the maximal averaged ictal EEG magnitude was a part of the visually defined onset zones in all cases. The ROC analysis demonstrated that electrodes showing >40% of the maximum of the EEG magnitude had a specificity of 0.95 and a sensitivity of 0.69 for concordance with visually defined onset electrodes as the gold standard, and that electrodes showing >30% of the maximum of the EEG magnitude had a specificity of 0.90 and a sensitivity of 0.74 (Fig. 3). Further change of the cutoff threshold from 30 to 20% did not increase the sensitivity (0.74–0.74) but considerably decreased the specificity (0.90–0.84) for the concordance with visually defined onset electrodes (Fig. 3). Retrospective visual EEG inspection using a time-cursor bar revealed that ictal discharges in the visually defined onset electrodes not showing >30% of the maximum of the averaged ictal EEG magnitude emerged somewhat later than the beginning of the first epoch (mean delay from the beginning of the first epoch±standard deviation: 0.5±0.3 s).

3.2. Topographic display of the sequential changes of the ictal EEG activity

Propagation of the ictal discharges could be delineated using the EEG magnitude within the same frequency band, up to the second epoch in 5/14 patients and up to the third epoch in 2/14

patients. In the remaining 7 patients, ictal propagation could not be delineated using the EEG magnitudes within the same frequency band only, since visual inspection revealed either the alteration of the frequency of ictal discharges, recruitment of rhythmic discharges at different frequency at different electrodes, or the contamination with movement artifacts. Alteration of the frequency of the ictal discharge frequency and recruitment of the rhythmic discharges at different frequency were delineated using the EEG magnitudes within multiple frequency bands (Fig. 2).

4. Discussion

The purpose in the present study was not to extract invisible EEG changes from the preictal state, but to represent the gradient of EEG magnitude at visible ictal onset. Quantitative ictal subdural EEG analysis was performed, using spectral analysis similar to that in previous reports (Alarcon et al., 1995; Gotman et al., 1993, 1995; Wu and Gotman, 1998), based on the assumption that epileptic seizures are represented as sustained and synchronized rhythmic ictal discharges with certain frequencies on the EEG (Lee et al., 2000) and that the ictal discharges within the first epoch are stationary. In short, the ictal EEG magnitude within a preset frequency band (including the ictal discharge frequency at the first epoch) was the main parameter on ictal EEG analysis in the present study. Topographic mapping of ictal EEG magnitude allows better visualization of spatial relationship with neuroimaging abnormalities. The results are reasonably consistent with ‘visually defined ictal EEG onset zone’.

The potential merits of the application of our quantitative method are described as follows. First, our method may provide more reproducible ictal EEG data in a clinical setting than the conventional visual inspection does. Second, better visualization of ictal EEG magnitude on topographic mapping may result in a significant reduction of the clinical workload, especially when the number of subdural electrodes exceeds 100 and the entire group of EEG traces are hardly delineated on the computer monitor with satisfactory resolution. Once the planar X-ray coordinate was registered into the Stellate digital system and the beginning of ictal discharges is visually identified in each seizure, the software can immediately create a topographic mapping of the ictal EEG magnitudes for consecutive epochs, regardless of the number of subdural grid electrodes. In addition, this quantitative method may be able to quantify the degree of ‘onset severity’. Some may hypothesize that a brain region showing the maximal ictal EEG magnitude has the highest density of synapses generating synchronized rhythmic seizure activity oriented to the subdural electrode plate, whereas those showing less ictal EEG magnitude have less synaptic potentials. Others may hypothesize that a brain region showing the maximal ictal EEG magnitude indeed initiates the seizure, whereas those regions showing less ictal EEG magnitude are recruited by seizure discharges somewhat later. In the present study, 26% of the visually defined onset electrodes were not detected by our quantitative EEG method, and the second review of conventional EEG recordings using a time-cursor bar revealed that ictal discharges in these electrodes emerged somewhat later than the beginning of the first epoch. Such minor discrepancy (‘onset’ versus ‘early spread’) would not have a clinical impact on determination of the resection margin in most cases, since it is generally assumed that epileptogenic cortex includes seizure-onset zones and regions consistently receiving early ictal propagation (Lüders et al., 1993). Visualization of onset severity might influence the clinical judgments in a subset of patients, in whom ictal discharges involve eloquent cortex and the surgical resection has to be limited by such cortex.

The limitations of the present study include the fact that our methodology is not totally independent from subjective interpretation by electroencephalographers. The epoch for quantitative analysis was placed at the very beginning of the visually defined ictal EEG onset. It has been reported that currently available automatic detection programs detect focal seizures with sensitivity of 90% (Gotman, 1990; Khan and Gotman, 2003), but such programs have not

been designed to detect the very beginning of seizures. The epoch of interest was not placed at the preictal state, since our main purpose of quantitative ictal subdural EEG analysis was to delineate the spatial gradient of the EEG magnitude at visible ictal onset, and not to extract an invisible EEG change during the preictal state. In the present study, the epoch of interest displaced 50 ms before or after the visible ictal onset did not make a significant change in the spatial pattern of ictal EEG magnitudes throughout the entire subdural electrodes. Furthermore, a previous study of spectral analysis for the ictal EEG suggested that an EEG change was detected 3 s earlier than visual examination in 30% of seizures starting gradually, but that gross disagreement was rare with respect to localization of the onset (Gotman et al., 1993).

Visualization of ictal propagation up to the third epoch using a single frequency band was not possible in the majority of patients in the present study, since recruitment of rhythmic discharges at quite diverse frequencies occurred as a seizure evolved. Therefore, multiple frequency bands should be taken into account to delineate the ictal discharge propagation. Although not seen in the present study, an ictal onset pattern with different frequencies at different electrodes would also require the multiple band frequency analysis (Blanke et al., 2000).

Different quantitative methods have been applied to preictal as well as ictal subdural EEG recordings. Since the purpose of each study is different from each other, it is unlikely that a single method is superior to others in every aspect. A voltage topographic mapping of the preictal spike activity was designed to visualize the origin of spikes preceding the clinical seizures in children with neocortical epilepsy (Otsubo et al., 2001). This method is simple and easy to conceptualize in patients showing preictal periodic spike activity as well as spike-wave activity. A voltage topographic mapping would be especially useful to delineate the source of spike activity in ictal EEG recordings consisting of a build-up of periodic spike activity at a frequency of <2 Hz without evolution into a continuous rhythmic activity. The wavelet transform method, which is one of non-stationary analyses, has been recently introduced for spectral analysis of the subdural as well as scalp EEG analysis (Adeli et al., 2003; Sun et al., 2001). This method consists of the short-time Fast Fourier Transform by adding the time-domain view (Akin, 2002). The wavelet analysis has been reported as a good method for analysis of spike-wave EEG onset pattern (Adeli et al., 2003), since this method takes into account time-varying spectral content of the signal within a window, which the Fast Fourier Transform ignores. Further exploration of the optimal quantitative method, using much larger samples of subjects, may increase the accuracy for delineating the epileptic focus.

Acknowledgements

This work was supported by NIH grants NS47550 (to E. A.), NS34488 (to H.T.C.) and NS38324 (to D.C.C.). We are grateful to Craig Watson, MD, PhD, Jagdish Shah, MD, Judy Ahn-Ewing, BA, R EEG/EP T, CNIM, Howard L. Wolfe, R EEG T, Carol Pawlak, R EEG T, Ann Atto, R EEG/EP T, Monica Adams, B.S.N., M.S.A., and the staff of the Division of Electroneurodiagnostics at Children's Hospital of Michigan, Wayne State University for the collaboration and assistance in performing the studies described above.

References

Adeli H, Zhou Z, Dadmehr N. Analysis of EEG records in an epileptic patient using wavelet transform. J Neurosci Methods 2003;123:69–87. [PubMed: 12581851]

Akin M. Comparison of wavelet transform and FFT methods in the analysis of EEG signals. J Med Syst 2002;26:241–7. [PubMed: 12018610]

Alarcon G, Binnie CD, Elwes RD, Polkey CE. Power spectrum and intracranial EEG patterns at seizure onset in partial epilepsy. Electroencephalogr Clin Neurophysiol 1995;94:326–37. [PubMed: 7774519]

Blanke O, Lantz G, Seeck M, Spinelli L, Grave de Peralta R, Thut G, Landis T, Michel CM. Temporal and spatial determination of EEG-seizure onset in the frequency domain. Clin Neurophysiol 2000;111:763–72. [PubMed: 10802445]

Chen LS, Otsubo H, Ochi A, Lai WW, Sutoyo D, Snead OC 3rd. Continuous potential display of ictal electrocorticography. J Clin Neurophysiol 2002;19:192–203. [PubMed: 12226564]

da Silva FL. EEG analysis: theory and practice. In: Niedermeyer E, da Silva FL, editors. Electroencephalography. Baltimore, MD: Williams and Wilkins; 1999, p. 1135–63.

Gotman J. Automatic seizure detection: improvements and evaluation. Electroencephalogr Clin Neurophysiol 1990;76:317–24. [PubMed: 1699724]

Gotman J, Levtova V, Farine B. Graphic representation of the EEG during epileptic seizures. Electroencephalogr Clin Neurophysiol 1993;87:206–14. [PubMed: 7691551]

Gotman J, Levtova V, Olivier A. Frequency of the electroencephalographic discharge in seizures of focal and widespread onset in intracerebral recordings. Epilepsia 1995;36:697–703. [PubMed: 7555988]

Jenssen S, Roberts C, Dlugos D, O'Connor MJ, Sperling MR. Patterns of intracranial seizure propagation. Epilepsia 2002;43(Suppl 7):222.

Khan YU, Gotman J. Wavelet based automatic seizure detection in intracerebral electroencephalogram. Clin Neurophysiol 2003;114:898–908. [PubMed: 12738437]

Lee SA, Spencer DD, Spencer SS. Intracranial EEG seizure-onset patterns in neocortical epilepsy. Epilepsia 2000;41:297–307. [PubMed: 10714401]

Lüders HO, Engel Jr. J, Munari C. In: Engel Jr. J, editor. Surgical treatment of epilepsies. New York: Raven Press; 1993, p. 137–53.

Otsubo H, Shirasawa A, Chitoku S, Rutka JT, Wilson SB, Snead OC 3rd. Computerized brain-surface voltage topographic mapping for localization of intracranial spikes from electrocorticography. Technical note J Neurosurg 2001;94:1005–9.

Spencer SS, Guimaraes P, Katz A, Kim J, Spencer D. Morphological patterns of seizures recorded intracranially. Epilepsia 1992;33:537–45. [PubMed: 1592034]

Sun M, Scheuer ML, Sclabassi RJ. Extraction and analysis of early ictal activity in subdural electroencephalogram. Ann Biomed Eng 2001;29:878–86. [PubMed: 11764318]

von Stockhausen HM, Thiel A, Herholz K, Pietrzyk U. A convenient method for topographical localization of intracranial electrodes with MRI and a conventional radiograph [Abstract]. Neuroimage 1997;5:S514.

Wellmer J, Von Oertzen J, Schaller C, Urbach H, Konig R, Widman G, Van Roost D, Elger CE. Digital photography and 3D MRI-based multimodal imaging for individualized planning of resective neocortical epilepsy surgery. Epilepsia 2002;43:1543–50. [PubMed: 12460257]

Wu L, Gotman J. Segmentation and classification of EEG during epileptic seizures. Electroencephalogr Clin Neurophysiol 1998;106:344–56. [PubMed: 9741763]

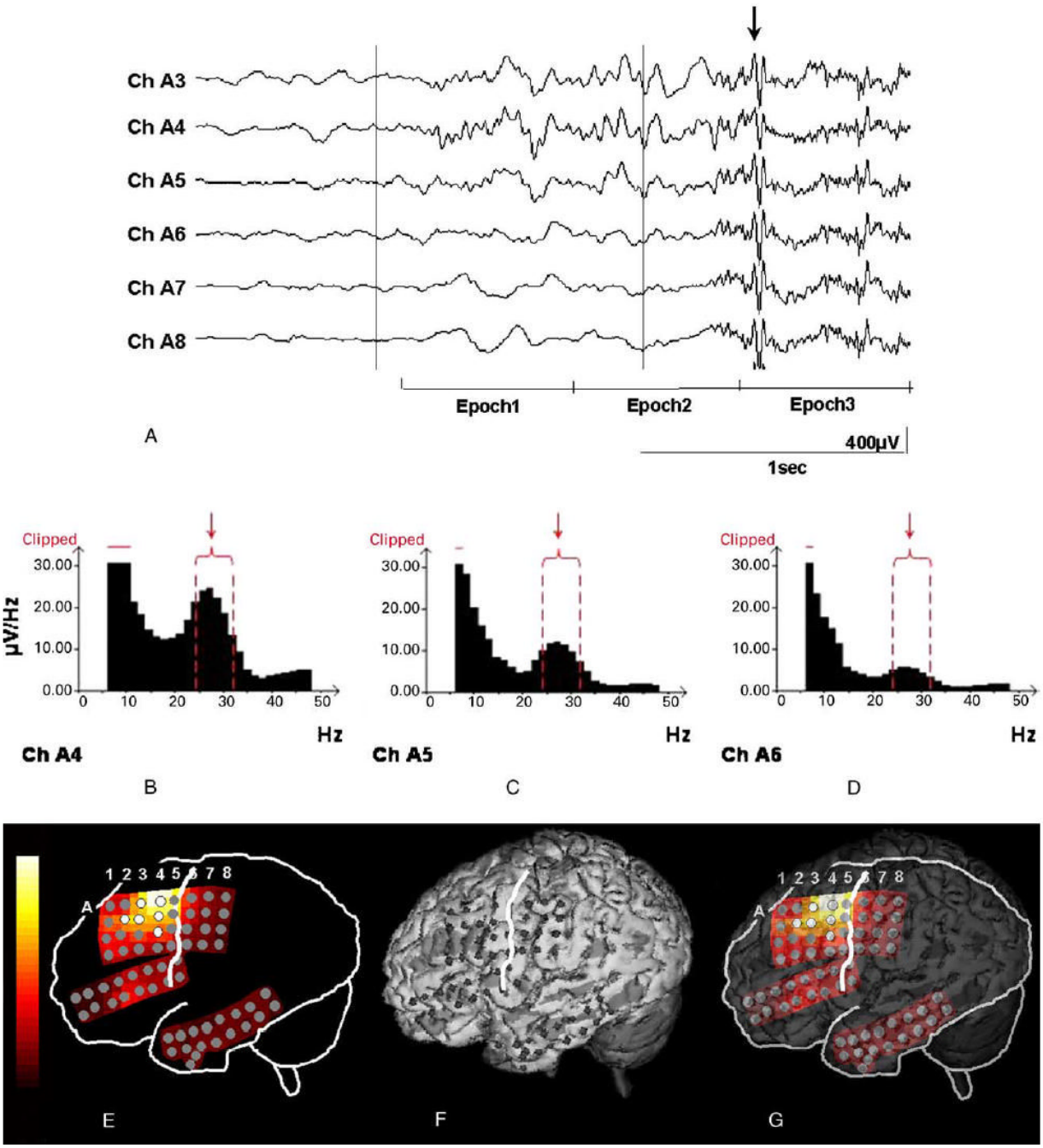

Fig. 1.

Ictal EEG of an 9-year-old boy with non-lesional neocortical epilepsy. (A) Prior to clinical onset (arrow), low-amplitude fast wave bursts emerge in channels A4, A3 and A5. The first epoch was placed at seizure onset, and the ictal discharge frequency was 26 Hz at the most-consistent onset electrode (A4). Each epoch length was 0.64 s. Note that EEG during epoch 3 was contaminated with diffuse movement artifacts (arrow). (B–D) Amplitude spectra at channels A4, A5 and A6 in the first epoch of the same ictal event are shown. A 5-point smoothing was applied. Ictal discharge frequency was 26 Hz at the first epoch. Note the various amplitudes of the peaks in the 24–32 Hz band at channels A4, A5 and A6, respectively (arrows) and that the lowest frequency part of the amplitude spectral curve is clipped off. (E) Topography

of the ictal EEG magnitude within a 24–32 Hz band at the first epoch in the same ictal event. The highest ictal EEG magnitude was seen at electrode A4. White electrodes represent 'visually defined onset' electrodes. (F) The location of subdural grid electrodes are displayed onto the 3D-reconstructed MRI (von Stockhausen et al., 1997). The white line represents the central sulcus. (G) The topography of the ictal EEG magnitude at seizure onset is superimposed onto the 3D-reconstructed MRI.

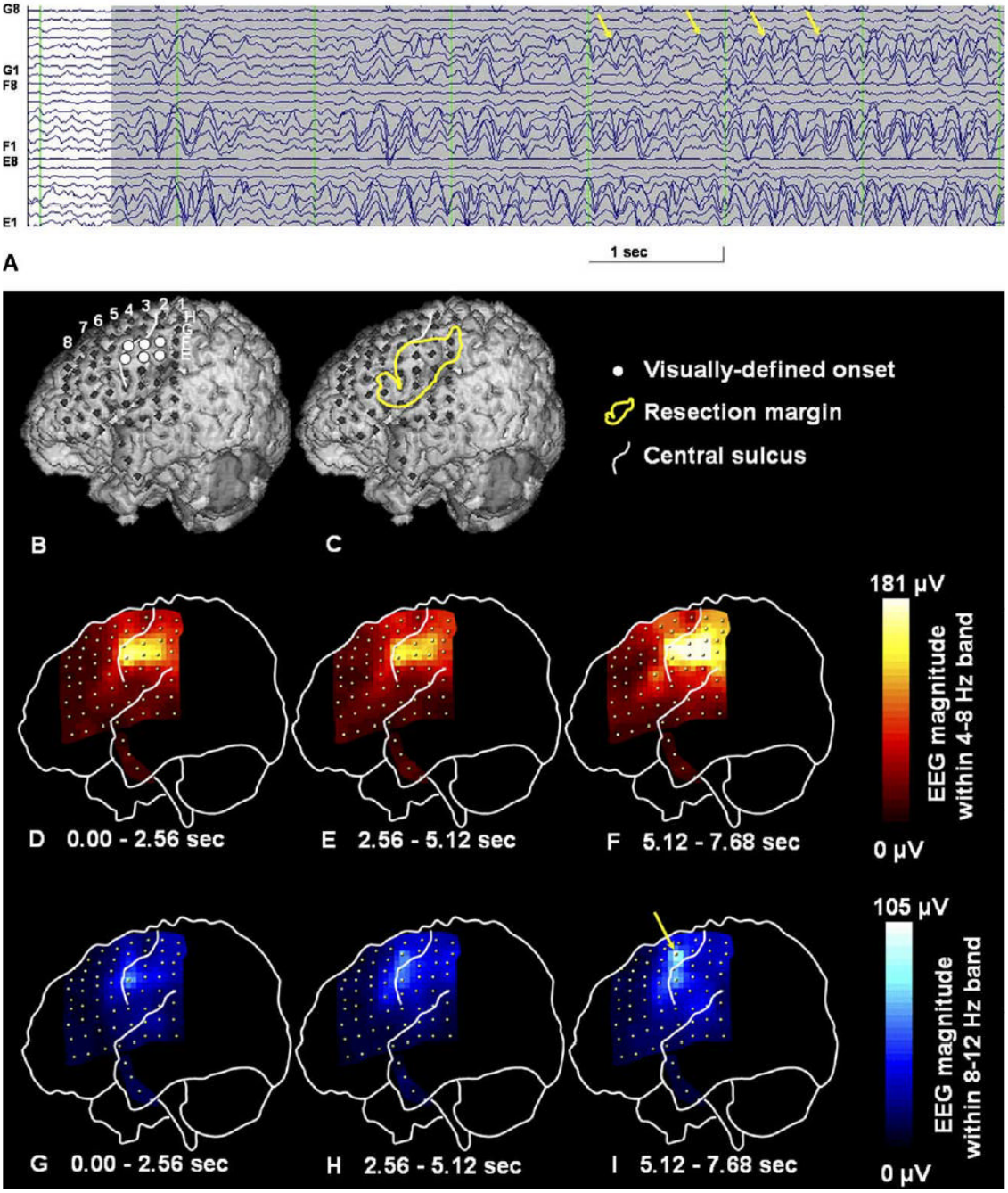

Fig. 2.

A 3D-reconstructed surface MRI and sequential topographic changes in the EEG magnitude during a seizure in a 1-year-old boy with uncontrolled focal seizures and a diagnosis of tuberous sclerosis complex. (A) A 7 s raw ictal subdural EEG showed a rhythmic theta activity at 5 Hz gradually building up in amplitude. Soon after the ictal EEG onset, brief rhythmic alpha wave activity emerged at electrode G4 and evolved into a continuous rhythmic alpha activity at the same area (arrows). This rhythmic alpha activity at electrode G4 may indicate ictal propagation. (B) The location of subdural electrodes is displayed onto the 3D MRI. Thereby, the visually defined ictal onset zones are shown by white circles. (C) The resection margin is delineated with a yellow line. The patient has been seizure-free for 12 months since surgery, where the

primary hand motor cortex under electrode G4 was not resected. (D–F) Spectral analysis for 3 consecutive 2.56 s epochs demonstrates the topography of EEG magnitudes within a 4–8 Hz frequency band and shows the highest EEG magnitude in the primary sensory face area at seizure onset. The EEG magnitude at that region was further increased in the subsequent epochs. Adjacent electrodes also show gradually increasing EEG magnitude in the subsequent epochs. (G–I) Spectral analysis for 3 consecutive 2.56 s epochs demonstrates the topography of EEG magnitudes within an 8–12 Hz frequency band, of which spatial pattern is similar to that for a 4–8 Hz frequency band at the first epoch. The EEG magnitude within an 8–12 Hz frequency band gradually increased especially at electrode G4 (arrow), as the rhythmic alpha wave activity became visually continuous during ictal propagation. At the third epoch, the EEG magnitude within an 8–12 Hz frequency band was considerably large and cannot be neglected to delineate the ictal propagation.

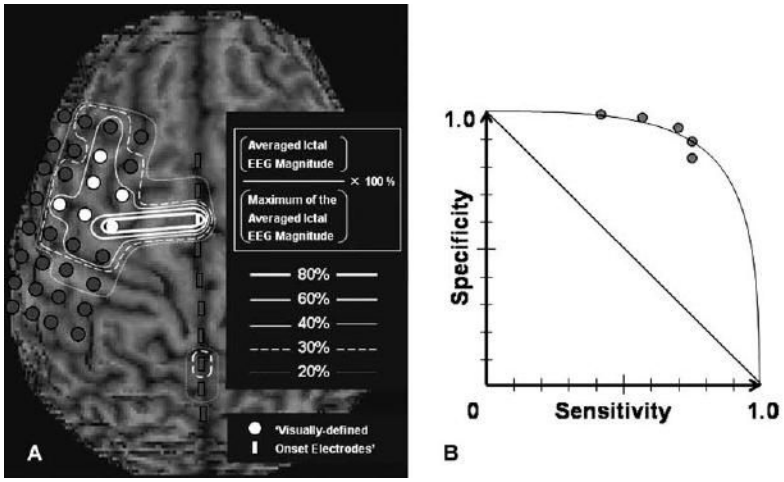

Fig. 3.

Concordance between quantitatively and visually defined onset electrodes. (A) The relationship between quantitatively and visually defined ictal onset zones in an 9-year-old boy with non-lesional neocortical epilepsy is shown (patient #7). It should be noted that subdural electrodes on the left inferior frontal or the temporal regions are not shown, and a total of 82 electrodes were included into statistical analysis. Electrodes encircled by bold, intermediate, thin, broken, and dotted lines represent the quantitatively defined ictal onset zones determined by various cutoff thresholds of 80, 60, 40, 30 and 20% of the maximal averaged ictal EEG magnitude. Cutoff thresholds of 80, 60, 40, 30 and 20% of the maximal averaged ictal EEG magnitude resulted in specificity of 1.00, 1.00, 0.96, 0.89, and 0.81 and sensitivity of 0.29, 0.29, 1.00, 1.00, and 1.00 for the concordance with 'visually defined onset' electrodes (white circles) in this individual. (B) The receiver operating characteristics curve (derived from mean specificity and sensitivity among all subjects) shows that cutoff thresholds of 80, 60, 40, 30 and 20% of the maximum of the averaged ictal EEG magnitude resulted in mean specificity of 1.00, 0.98, 0.95, 0.90 and 0.84 as well as mean sensitivity of 0.41, 0.56, 0.69, 0.74 and 0.74 for the concordance with 'visually defined onset' electrodes. Three patients showed multiple ictal onset foci; in these cases, we calculated sensitivity and specificity of the quantitatively defined seizure-onset zone for concordance with the dominant focus.

Table 1

Summary of clinical information

Gender/ age (yr)	Scalp ictal EEG onset	MRI	Subdural electrode placement	Subdural ictal EEG onset	Latency between ictal EEG onset and clinical onset	Cortical resection	Surgical outcome
1. M/1	L P–C	Cortical tubers	L P–F–T	L P–F	10–30 s	L P–F	Seizure-free
2. M/5	L F–C	Subcortical heterotopias	L F–P–T	L F	2–5 s	L F	Seizure-free
3. M/5	L O–T–P	Pachygyria	L O–T–P–F	L O–T	Difficult to determine (insidious clinical onset)	L O–T–P	Rare residual seizures
4. M/6	Midline (Cz)	Normal	L F–P–T	L F	2–5 s	L F	Seizure-free
5. F/7	L C–P	Normal	L P–T–F	L P	10–30 s	L P–T	50% Reduction
6. F/8	R F–C	Normal	R F–T–P	R F	<2 s	R F–T–P	Seizure-free
7. M/9	L F	Normal	L P–F–T	L F	<2 s	L F	Seizure-free
8. F/9	L C–P–T	Cortical tuber	L F–P–T	L F–P	<2 s	L F–P–T	>90% Reduction
9. M/11	Not detectable	Brain tumor	L F–P	L F	5–30 s	Lesionectomy at L precentral gyrus	Seizure-free
10. M/11	R T	Brain tumor	R T–O–P–F	R T–O	5–20 s	R T–O	Seizure-free
11. M/12	R F–C	Porencephaly	R F–T–P	R F	5–20 s	R F–T	Seizure-free
12. M/14	R T–F	Normal	R T–P–F	R P	2–5 s	R P–T	Seizure-free
13. M/15	R T	Polymicrogyria	R T–P–F	R T	Difficult to determine (insidious clinical onset)	R T–P	>90% Reduction
14. M/16	R Hemisphere	Infarction	R T–O–P–F	R O–T	2–5 s	R Subtotal hemispherectomy	Seizure-free

F, female; M, male; R, right; L, left; F, frontal, T, temporal; C, central; P, parietal; O, occipital.